Trichromatic thermoreflectometry for an improved accuracy of true temperature field measurement on a multi-material part

Thierry Sentenac, Rémi Gilblas, Florian Bugarin

Trichromatic thermoreflectometry for an improved accuracy of true temperature field measurement on a multi-material part

T. Sentenac*, R. Gilblas, F. Bugarin

Institut Clément Ader (ICA), Université de Toulouse, CNRS, Mines Albi, UPS, INSA, ISAE-SUPAERO, Campus Jarlard, F-81013 Albi CT Cedex 09, France

A B S T R A C T

This article addresses the problem of measuring an accurate temperature field on a multi-material part which exhibits spatial, temporal, spectral and thermal emissivity variations. The article analyses the contribution of trichromatic thermoreflectometry method compared to bichromatic thermoreflectometry method. Thermoreflectometry, an active thermography method, measures in-situ the emissivity, together with the temperature. The emissivity is measured indirectly by measuring the bidirectional reflectivity of the sample and by estimating its diffusion function. The bichromatic thermoreflectometry assumes an independent diffusion function with wavelength. For trichromatic thermoreflectometry, the diffusion function varies linearly with the wavelength. This article demonstrates the benefit of trichromatic thermoreflectometry on both simulated and experimental data. The simulated data come from measurements of emissivity and diffusion function of six different materials (metallic and dielectric) performed with a FTIR (Fourier Transform InfraRed) spectrometer. The addition of noise on these estimated values enables the propagation of uncertainties, which shows that the bias on temperature estimation is lower with trichromatic thermoreflectometry. Finally, an experimental demonstration on three of the six materials confirms a lower temperature measurement error (difference between the measured temperature and a reference temperature) with trichromatic thermoreflectometry.

Keywords:
Thermoreflectometry
Active thermography
Thermal measurement
Emissivity modelling
Metallic and dielectric materials

1. Introduction

For many industrial processes in energy [1], aeronautical engineering [2], automotive engineering [3] or microelectronics [4], thermal diagnostics is a key physical parameter for their design, monitoring and control, as well as for the durability of their associated components. These components may be furnaces, nuclear reactors or aircraft engines, which often operate at high temperatures with strong thermal gradients. Their surfaces are often oxidised and possibly deteriorated due to severe operating conditions. The materials used for these components are often heterogeneous multi-materials, since they need to possess different thermal strain and thermal shock resistance due to high heat transfers on their surfaces. These different materials provide a proper balance of the mechanical and thermal properties depending on where the stresses are applied.

In most of these components, thermal diagnostics must be carried out without direct instrumentation and must be performed remotely and in real time with a low intrusiveness to avoid damage. On-line, surface and remote thermal measurements can only be performed by optical radiation methods operating in two dimensions, such as thermography. These radiative temperature measurement methods have the capability to provide a full field temperature measurement on large surfaces, in real time, over a wide temperature range and with high accuracy, but they require the knowledge of the surface emissivity. For a multi-material component, the main issue is thus to investigate a radiative measurement method capable of taking into account the spatial, temporal, spectral and thermal variations of the emissivity.

Radiative temperature measurement methods usually fall into two categories, passive and active [5]. Passive methods make assumptions for overcoming, reducing or correcting the influence of emissivity. Monochromatic thermography operates at specific wavelengths (Christiansen's wavelength for ceramic material [6] or χ wavelength for metallic material [7]) or spectral bands [8–10] where the emissivity can be considered as independent of wavelength or temperature or surface conditions. These methods operate in lab conditions with a controlled environment but they cannot take into account the variations over time of thermo-optical properties, for example due to a contamination by exhaust gasses or oxidation phenomena. Polychromatic thermography [11–13] models the evolution of the emissivity as a function of the wavelength and solves a system of equations whose number depends on the number of parameters of the model. One difficulty [14] is the choice of the wavelengths, which is based on the following trade off: close

* Corresponding author.
E-mail address: sentenac@laas.fr (T. Sentenac).

enough to overcome emissivity variations and far away enough to optimise the conditioning of the equations system and therefore to decrease the uncertainty of the calculated true temperature [15]. On a multi-material component with the radiative properties varying over time, another difficulty is to design emissivity modelling that is valid for the different radiative behaviour of the various materials of the component, but also robust enough over time to take into account the changes in the surface conditions. The second category of methods, active methods, is divided into two classes, direct and indirect methods. Direct methods, such as photothermal thermography, aim to measure the emissivity or, more precisely, the absorptivity [16], or both emissivity and radiance temperature [17], by applying thermal, optical or mechanical stress to the surface of materials. The local heating applied on the material can require high power for high-temperature components. The indirect active method consists in measuring the reflectance of the material illuminated by a source of lower power [18]. Rather than measuring reflectance, another solution only measures the bidirectional reflectivity [19], which is easier to grasp with an active thermography system, called thermoreflectometry. This method performs simultaneous measurements of the sample thermal signal through the radiance temperature (thermography) and of its emissivity with a bidirectional reflectivity measurement (reflectometry) instead of a reflectance measurement. The relationship between bidirectional reflectivity and reflectance is the integral of the reflection indicator function on the solid angle formed by the surface of the measured surface component. The method is then based on two steps. The first step is the approximation of the integral by a model function of n parameters versus the wavelength, which is called the diffusion function. The next step is the resolution of a system composed of $n + 1$ polychromatic radiometric equations, including diffusion model parameters and measurements of radiance temperatures and bidirectional reflectivities at different wavelengths. The resolution of radiometric equations provides the true temperature and the n model parameters of the diffusion function. Bichromatic thermoreflectometry [19] assumes that the diffusion function is only a constant over a given spectral range. This assumption means that the reflectivities are homothetic at two wavelengths. The method has the capability to measure true temperature fields on a multi-material part [20] with spatial, temporal, spectral and thermal emissivity variations thanks to the in situ and simultaneous measurement of emissivity and radiance temperature. However, the assumption of a constant diffusion function can be restrictive, particularly in the case of spectral behaviour of materials whose reflectance decreases slightly with wavelength.

This paper introduces trichromatic thermoreflectometry, which models the diffusion function with a linear function of the wavelength and provides the true temperature by solving a system of three radiometric equations at three wavelengths. This article aims to demonstrate that trichromatic thermoreflectometry addresses all cases of reflectance behaviours of opaque materials. This linear function of the diffusion function has the ability to take into account all emissivity behaviours, whereas polychromatic thermography methods involve the use of complex emissivity models. The paper also argues that the introduction of a third wavelength improves the convergence of the resolution method of the system. The residual of calculated true temperature is thus lower and therefore the temperature uncertainty is reduced for all cases of measurement. A comparison of the temperature measurement error (difference between the calculated temperature and a reference temperature) between bichromatic and trichromatic thermoreflectometry highlights the contribution of trichromatic reflectometry to the decrease in temperature error. The temperature error is analysed for metallic materials (tungsten, inconel, copper) with different surface finishes and for dielectric materials (dysprosium and erbium oxides) with a selective spectral behaviour. The comparison is carried out on one hand with simulated data resulting from the optical properties measured on these materials and on the other hand from measurements performed on a multi-material part. This part is composed of different metallic and dielectric materials. The benefits of trichromatic thermoreflectometry are analysed across the range of spectral behaviours of the materials.

The paper is organised as follows. Section 2 is dedicated to the theoretical basis and assumptions of thermoreflectometry and highlights the diffusion function modelling. This modelling is carried out thanks to thermo-optical properties, emissivity and bidirectional reflectivity, measured on various metallic and dielectric materials. Section 3 provides a simulation approach based on the previous database, to analyse the temperature error introduced by bichromatic and trichromatic thermoreflectometry. Section 4 is devoted to the comparison of a bi- and trichromatic thermorefletometer and presents their true temperature field measurements carried out on large area of a multi-material part without any knowledge or assumption about the material's emissivity.

2. Definition and physical principle of thermoreflectometry

The section describes the principle of thermoreflectometry, which is deduced from the measurements at different wavelengths of the bidirectional reflectivities and from a modelling of the relative diffusion of the material surface. The section concludes with a description of the system composed of polychromatic radiometric equations, including diffusion function parameters and measurements of radiance temperatures and bidirectional reflectivities at different wavelengths.

2.1. Principle of thermoreflectometry

For an opaque material and following Kirchhoff's laws, the directional spectral emissivity, $\varepsilon^{\vec{r}_0}$, and the spectral reflectance, $\rho^{\vec{r}_0,\cap}$, obey the following equation:

$$\varepsilon^{\vec{r}_0}(\lambda, T) = 1 - \rho^{\vec{r}_0,\cap}(\lambda, T) \tag{1}$$

The reflectance is given by the integration in all directions $\vec{x}$ of the bidirectional reflectivity, which is carried out over the upward hemisphere, as follows:

$$\rho^{\vec{r}_0,\cap}(\lambda, T) = \int_{\Omega_x=2\pi} \rho^{\vec{r}_0,\vec{x}}(\lambda, T)\cos(\theta_x)d\Omega_x \tag{2}$$

The first step is the introduction of the measured bidirectional reflectivity in a single direction $\vec{x}_0$, denoted by $\rho^{\vec{r}_0,\vec{x}_0}$. The reflectance is then expressed with respect to the measured bidirectional reflectivity, as follows:

$$\rho^{\vec{r}_0,\cap}(\lambda, T) = \rho^{\vec{r}_0,\vec{x}_0}(\lambda, T) \int_{\Omega_x=2\pi} f^{\vec{r}_0,\vec{x},\vec{x}_0}(\lambda, T)\cos(\theta_x)d\Omega_x \tag{3}$$

where $f^{\vec{r}_0,\vec{x},\vec{x}_0}$ is the reflection polar angle variation, which represents normalised values of bidirectional reflectivities.

The second step is the introduction of the diffusion function, denoted by $\eta(\lambda, T)$, as an unknown bivariate function of the wavelength and the temperature, which represents the previous integral as follows:

$$\eta^{\vec{r}_0,\vec{x}_0}(\lambda, T) = \int_{\Omega_r=2\pi} f^{\vec{r}_0,\vec{x},\vec{x}_0}(\lambda, T)\cos(\theta_x)d\Omega_x \tag{4}$$

Indeed, $f^{\vec{r}_0,\vec{x},\vec{x}_0} = \frac{\rho^{\vec{r}_0,\vec{x}}(\lambda,T)}{\rho^{\vec{r}_0,\vec{x}_0}(\lambda,T)}$ (where $\rho^{\vec{r}_0,\vec{x}_0}$ is the bidirectional reflectivity in the incident direction r_0 and reflected direction x_0) is bounded and differentiable, while the integral is also differentiable. The integral has regularity properties to justify its interpolation using a regular polynomial function. This function, defined by the diffusion function, is related to the shape of the normalised reflection of the material (diffuse or specular). It is therefore only geometrical and can be associated to a shape factor which represents the volume of the bidirectional reflectivities normalised in the reference direction $\vec{x}_0$. If this direction corresponds to the maximum of reflection, the polar angle

variation is then between 0 and 1. Its integral (see equation (3)), the diffusion function, varies between 0 and π. Low values characterise rather specular materials with a polar angle variation which is very narrow around a privileged direction. High values are obtained for Lambertian materials with high values of the polar angle variation.

According to equations (1), (3) and (4) and thanks to Helmholtz's reciprocity theorem applied to bidirectional reflectivity, $\rho^{\vec{r}_0,\vec{x}_0}$, the emissivity is then expressed as a function of the measured bidirectional reflectivity in a single direction $\vec{x}_0$ and the unknown diffusion function, as follows:

$$\varepsilon^{\vec{r}_0}(\lambda, T) = 1 - \rho^{\vec{x}_0,\vec{r}_0}(\lambda, T)\eta^{\vec{r}_0,\vec{x}_0}(\lambda, T) \tag{5}$$

Equation (5) shows that emissivity has a physical sense only if the diffusion function is positive and less than $1/\rho^{\vec{x}_0,\vec{r}_0}$.

The third step is the resolution of a polychromatic system of radiometric equations. This equation connects the object measured radiance, L, at temperature T to the black body radiance, L_0, at radiance temperature T_R. The latter is also equal to the product of the emissivity, ε, by the black body radiance calculated at temperature T. If the emissivity is replaced by equation (5), the polychromatic system for different λ_i is then given by the following equation:

$$L_0\left(\lambda_i, T_R^{\vec{r}_0}(\lambda_i)\right) = \left(1 - \rho^{\vec{x}_0,\vec{r}_0}(\lambda_i, T)\eta^{\vec{r}_0,\vec{x}_0}(\lambda_i, T)\right)L_0(\lambda_i, T) \tag{6}$$

The black body radiance, L_0, is expressed following the Wien's approximation (see equation (7)), accurate to within 1% if the condition $\lambda\ T_R < 3000\mu mK$ is observed (i.e. wavelength λ lower than $2.4\mu m$ for a radiance temperature range T_R of $300 - 1000°C$).

$$L_0(\lambda_i, T) = C_1\lambda_i^{-5}exp\left(\frac{-C_2}{\lambda_i T}\right) \tag{7}$$

System (6) is rewritten including equation (7) and according to equation (8).

$$\frac{1}{T} = \frac{1}{T_R^{\vec{r}_0}(\lambda_i)} + \frac{\lambda_i}{C_2}\ln\left(1 - \rho^{\vec{x}_0,\vec{r}_0}(\lambda_i, T)\,\eta^{\vec{r}_0,\vec{x}_0}(\lambda_i, T)\right) \tag{8}$$

The unknown parameters of equations (6) or (8) are the true temperature and the diffusion function at different wavelengths. As the number of unknowns is greater than the number of equations, the resolution of this system involves modelling the diffusion function with respect to the wavelength.

2.2. Modelling of diffusion function in near-infrared spectral band

The fourth step is the discussion about the diffusion function modelling in the near-infrared spectral band. This discussion is carried out from a database of thermo-optical properties, emissivity and bidirectional reflectivity measured in the near-infrared spectral band, which is very representative of various spectral behaviours of metallic and dielectric materials.

2.2.1. Discussions on measured emissivity behaviour of selected materials in the database

The directional spectral emissivity values of the selected samples are evaluated indirectly through the measurement of directional hemispherical reflectivity (see equation (1)), performed by a Fourier transform spectrometer equipped with an integrating sphere. The values, provided at room temperature and for a direction of 13°, are plotted in Fig. 1.

As shown in Fig. 1, with emissivity values from 0.4 to 0.9 and emissivity variations both increasing and decreasing, the database addresses all spectral emissivity behaviours. Oxidised copper, tungsten and stainless steel exhibit a metal-like behaviour, with emissivity decreasing with wavelength. Inconel is a material with a very low emissivity decrease, which behaves as a grey body. Moreover, inconel, with its high emissivity value, provides a measurement case of a low value of

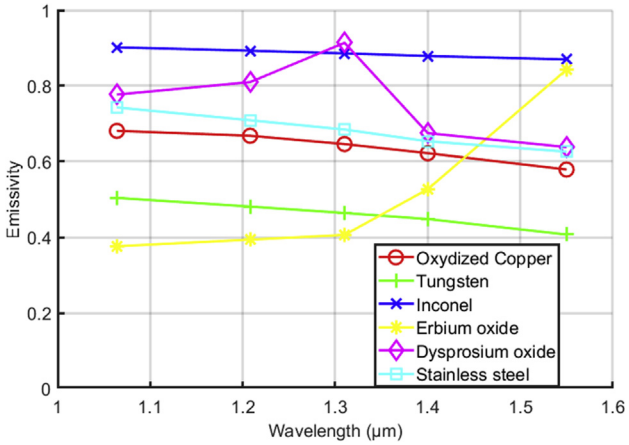

Fig. 1. Emissivities of selected materials of database versus near infrared wavelengths.

reflectance, which can be challenging for the thermoreflectometry method. Dysprosium and erbium oxides have a spectrally selective behaviour with high variations of emissivity. They constitute the most difficult measurement case for conventional thermography methods.

2.2.2. Discussions on diffusion function variations of selected materials in the database

The bidirectional reflectivities were also measured with the Fourier transform spectrometer, equipped with a goniometer enabling the measurement of reflectivity in the incidence plane for a given incident angle equal to 13° and for several reflection angles. An example of normalised bidirectional reflectivity ($\frac{\rho^{\vec{x}_0,\vec{r}_0}}{\rho^{\vec{r}_0,\vec{r}_0}}$) variations versus the angle is provided in Fig. 2 for the dysprosium oxide and the stainless Steel case.

This figure clearly shows the different behaviours between the metallic and dielectric materials. The stainless steel samples scatters less than the dysprosium Oxide. Using these measurements, performed at room temperature, and equation (4), the diffusion function values are calculated and plotted in Fig. 3. A hypothesis of orthotropy around the Snell-Descartes direction is made because of the incapacity for the goniometer to measure out-of-plane reflexions.

The values of the diffusion function vary between 0.9 and 2.6 and show materials with specular and diffusive behaviours due to different surface finishes. For specular materials, for example tungsten or stainless steel with a polished surface, the diffusion function value is low and

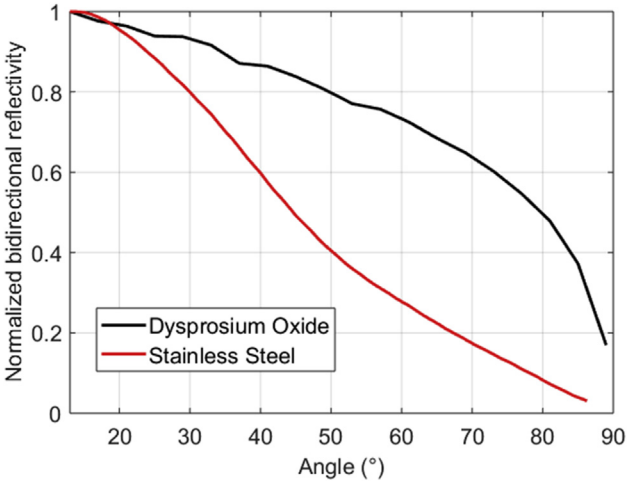

Fig. 2. Normalised bidirectional reflectivities versus the angle for the dysprosium oxide and the stainless steel case.

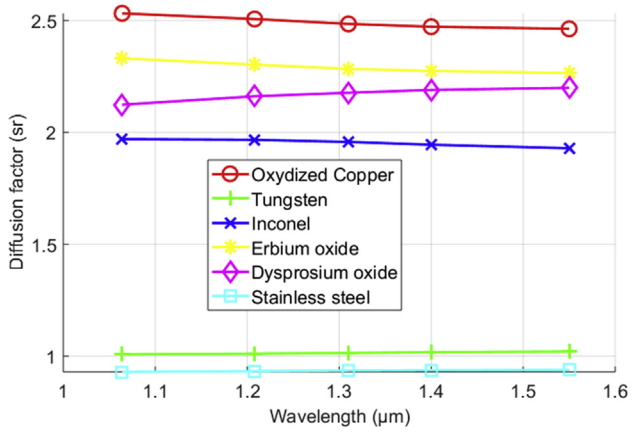

Fig. 3. Diffusion function values of selected materials of database versus near infrared wavelengths.

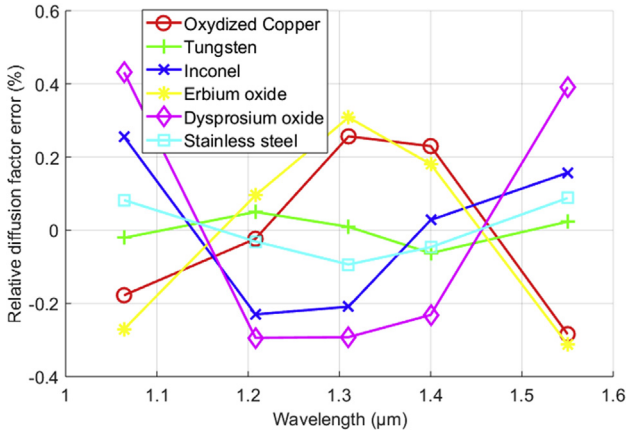

Fig. 4. Relative interpolation error of diffusion function versus wavelength.

close to 1. In contrast, for diffuse materials (oxidised copper, dysprosium and erbium oxides with a rougher surface), the values of the diffusion function are high and little less than π. Metallic materials (oxidised copper, inconel, tungsten and stainless steel) show a decreasing emissivity and both a decreasing and increasing diffusion function with the wavelength. Erbium oxide shows emissivity that increases with the wavelength and diffusion function values that decrease with the wavelength. Finally, the emissivity of dysprosium oxide is both increasing and decreasing, but the value of the diffusion function is always increasing. The database demonstrates materials with different behaviours of emissivity and diffusion function.

We notice that the evolution of the diffusion function with the wavelength is much lower than the emissivity one. For materials with a very low variation of diffusion function (tungsten and stainless steel), a diffusion function modelling, $\hat{\eta}$, defined as constant value relative to the wavelength can be justified in the spectral band studied. The diffusion model is then expressed as follows:

$$\hat{\eta}^{\vec{r_0},\vec{x_0}}(\lambda_i, T) = \hat{\eta}^{\vec{r_0},\vec{x_0}}(T) = \eta_0(T) \tag{9}$$

This model of a diffusion function independent of the wavelength makes it possible to solve the polychromatic system of equation (6) with only two wavelengths (λ_1, λ_2). Following equations (3) and (4), this model makes it possible to write that the ratios at the two wavelengths of the bidirectional reflectivities and the reflectance are equal, as shown by the following equation:

$$\frac{\rho^{\vec{x_0},\vec{r_0}}(\lambda_1)}{\rho^{\vec{x_0},\vec{r_0}}(\lambda_2)} = \frac{\rho^{\vec{r_0},\cap}(\lambda_1)}{\rho^{\vec{r_0},\cap}(\lambda_2)} = \frac{1-\varepsilon^{\vec{r_0}}(\lambda_1, T)}{1-\varepsilon^{\vec{r_0}}(\lambda_2, T)} \tag{10}$$

Equation (10) means that the reflectivity is strictly homothetic at the two wavelengths. This formulation is therefore much less restrictive than the usual hypothesis of the grey body found by bichromatic thermography, which assumes the equality of the reflectances at two wavelengths.

For materials with a higher variation of the diffusion function (Oxidised copper, erbium and dysprosium oxides), a linear diffusion function modelling versus the wavelength is required to limit the modelling error. This model is then written for a given temperature T and a wavelength λ according to equation (11).

$$\hat{\eta}^{\vec{r_0},\vec{x_0}}(\lambda, T) = \eta_0(T) + \eta_1(T) \times \lambda \tag{11}$$

The polychromatic system (6) has a maximum of three radiometric equations to estimate the true temperature and the two parameters of the diffusion function. As shown in Fig. 4, the model of equation (11) introduces a relative interpolation error, $E_\eta = \frac{\eta(\lambda)-\hat{\eta}(\lambda)}{\eta(\lambda)} = \frac{\Delta\eta}{\eta}$, of less than 0.5 %.

Even in the case of materials with a low variation of the diffusion function, a linear variation model with the wavelength reduces the relative error $\frac{\Delta\eta}{\eta}$ of a ratio of 5 compared to a model independent of the wavelength. The impact of the diffusion function modelling on the temperature error is analysed in the next section.

3. Contributions of trichromatic thermoreflectometry on the accuracy of true temperature measurement

This section is devoted to the comparison of the true temperature error obtained with tri- and bichromatic thermoreflectometry. This comparison is based on noisy simulated inputs (radiance temperature and bidirectional reflectivity) calculated with the properties of the previous database. The error between estimated outputs (true temperature and diffusion function) and the outputs used to generate the simulated inputs is then calculated. The true temperature error is the criterion for evaluating and comparing the methods.

The simulation method to generate the noisy inputs (radiance temperature and bidirectional reflectivity) is first detailed. The criterion of true temperature error is then explained. Finally, true temperature errors with tri- and bichromatic thermoreflectometry are investigated.

3.1. Simulation procedure

3.1.1. Calculation of the noisy simulated inputs

The two inputs I of the thermoreflectometry method are the radiance temperature (T_R) and the bidirectional reflectivity ($\rho^{\vec{x_0},\vec{r_0}}$). For a true temperature T of 500°C and from the emissivity values of the database (see Fig. 1), the radiance temperature (T_R) is calculated using equation (8). From emissivity and diffusion-function values of the database (see Fig. 3) and according to equation (5), the bidirectional reflectivity ($\rho^{\vec{x_0},\vec{r_0}}$) is calculated. These inputs I of the thermoreflectometry method are plotted in Fig. 5 for each wavelength and each material selected in the database.

The variations of the radiance temperature values relative to the wavelength follow the emissivity ones (see Fig. 1). According to equation (8), the values of radiance temperatures are always lower than the true temperature of 500°C. In contrast, the variations of bidirectional reflectivities are inverted compared to emissivity variations. The highest value of reflectivity is recorded for tungsten, due to its specular behaviour. For oxidised copper, tungsten, stainless steel and inconel, the two inputs vary in opposite directions: the value of the bidirectional reflectivity decreases and the value of the radiance temperature increases. For dysprosium oxide, the two inputs also vary in the opposite direction. For erbium oxide, the two inputs vary in the opposite and in the same direction. Both behaviours are observed.

A noise value derived from a Gaussian distribution $\mathcal{N}(0, \sigma_I^2)$ of mean zero and standard deviation σ_I is added to each input I according

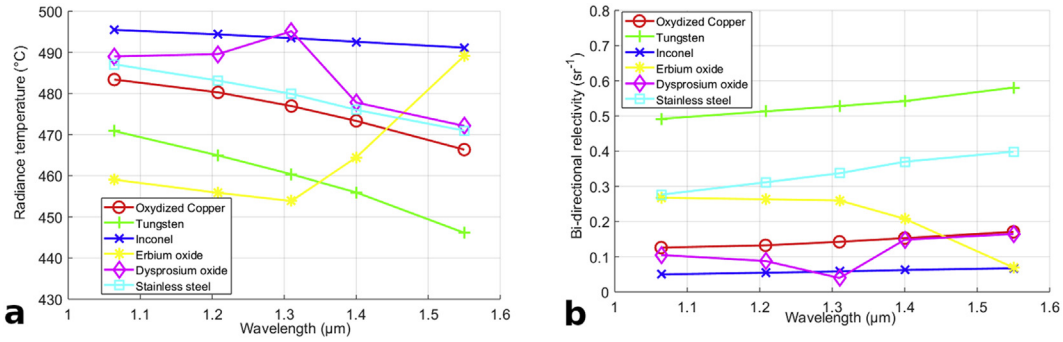

Fig. 5. Radiance temperature T_R (a) and bidirectional reflectivity $\rho^{\vec{x_0},\vec{r_0}}$ (b) of the selected materials of the database versus near infrared wavelengths.

to the following equation:

$$\check{I}_j = I_j + \nu_j \tag{12}$$

where ν is the j^{th} trial value of N trials ($j = 1...N$).

3.1.2. System resolution

The resolution of system (8) is performed by an optimisation algorithm based on the "fsolve" MATLAB function, using the Trust Region Dogleg Algorithm. This algorithm combines a Quasi-Newtonian method and a trust region method. The initial values of system parameters are given as follows: (a) according to equation (8), true temperature is always higher than radiance temperature. So the initial true temperature T_0 is set to the highest value of radiance temperature $T_0 = max(T_R(\lambda_i))$; (b) according to equation (5), the diffusion function must be lower than the inverse of bidirectional reflectivity. So its initial value is $1/(max(\rho^{\vec{x_0},\vec{r_0}}(\lambda_i))$.

The resolution gives an estimated true temperature $\hat{T}$ and the parameters of the diffusion function $\hat{\eta}$.

3.1.3. Evaluation criteria

Performances of the bi- and trichromatic thermoreflectometry method are quantified by computing the usual absolute error of temperature: $E_T = \|T - \hat{T}\|$ where the " ˆ " notation represents the estimated value. For errors measured with j noisy data, the mean value $\bar{E}_T$ and the standard deviation σ_{E_T} of the absolute temperature error are calculated on the N trials. The mean value $\bar{E}_T$ of true temperature error is the bias on true temperature).

3.1.4. Simulation conditions

The noisy inputs were processed thanks to equation (12) on a number N of 500 trials and with a noise standard deviation of radiance temperature σ_{T_R} (respectively bidirectional reflectivity σ_ρ) from a minimal value, $\sigma_{T_{R_{min}}}$, of 0 to a maximal value, $\sigma_{T_{R_{max}}}$, of $5°C$ (respectively from $\sigma_{\rho_{min}}$ of 0 to $\sigma_{\rho_{max}}$ of $0.01sr^{-1}$).

The normalised standard deviation on the inputs, denoted $\sigma_{I_{rel}}$, is calculated with the following equation:

$$\sigma_{I_{rel}}(\%) = \frac{100}{2} * \left(\frac{\sigma_{T_R} - \sigma_{T_{R_{min}}}}{\sigma_{T_{R_{max}}} - \sigma_{T_{R_{min}}}} + \frac{\sigma_\rho - \sigma_{\rho_{min}}}{\sigma_{\rho_{max}} - \sigma_{\rho_{min}}} \right) \tag{13}$$

A value of 100% of the normalised standard deviation $\sigma_{I_{rel}}$ means a standard deviation on radiance temperature of $5°C$ and a standard deviation on bidirectional reflectivity of $0.01sr^{-1}$.

3.2. Temperature error with trichromatic thermoreflectometry method

For the wavelengths combination ($\lambda_1 = 1.064$, $\lambda_2 = 1.310$ and $\lambda_3 = 1.550\mu m$), the mean value, $\bar{E}_T$, and the standard deviation σ_{E_T} of temperature error of trichromatic thermoreflectometry is plotted in Fig. 6 versus the normalised standard deviation on the inputs $\sigma_{I_{rel}}$.

The figure shows that the evolution of the mean value ($\bar{E}_T$) and the standard deviation (σ_{E_T}) of temperature error tends to 0 when the standard deviation on the inputs also tends to 0. Without noise on the inputs, the estimated temperature of the trichromatic thermoreflectometry is the true temperature. The system resolution with three equations does not generate any bias.

Moreover, despite the two behaviours of the diffusion function showed on the selected materials of the database and in Fig. 3, a similar behaviour is observed on the mean and the standard deviation of the temperature error. They only increase linearly with the standard deviation on the noise added to the inputs.

Fig. 7 displays the mean value of the estimated coefficient η_1 of the diffusion function modelling $\hat{\eta} = \eta_0 + \eta_1 \times \lambda$, given in equation (11), over the five hundred trials. In coherence with Fig. 4, the values of coefficient η_1 go to zero for materials tungsten and stainless steel with a diffusion function which is almost constant. In addition, the value of coefficient η_1 is negative (respectively positive) for oxidised copper and erbium oxide materials (respectively for dysprosium oxide). The values of the estimated coefficient η_1 are consistent with the measured values of Fig. 3. The modelling of the diffusion function by a linear model presented in equation (11) gives a good description of the behaviour of the diffusion function.

Finally, a temperature error of less than $1°C$ is obtained with a normalised standard deviation $\sigma_{I_{rel}}$ of 15% (i.e. a standard deviation on radiance temperature (respectively on the bidirectional reflectivity) of $0.75°C$ (respectively of $0.0015\ sr^{-1}$)). These values of noise standard deviation on radiance temperature and on reflectivity measurements are reachable values in real experimental conditions. The trichromatic thermoreflectometry method therefore has the potential to provide a true temperature error of 0.2%.

3.3. Temperature error with bichromatic thermoreflectometry method

The three wavelengths of trichromatic thermoreflectometry provide three possible pairs of wavelengths for bichromatic thermoreflectometry (λ_1-λ_2; λ_1-λ_3 and λ_2-λ_3). For these three wavelength pairs and with the same simulation conditions as the trichromatic thermoreflectometry, the mean temperature error $\bar{E}_T$ relative to normalised standard deviation $\sigma_{I_{rel}}$ is plotted in Fig. 8.

This figure shows that the temperature error depends on the choice of the wavelength pairs. To take an example, Fig. 8 (a), with a choice of wavelength λ_1-λ_2, shows a large temperature error (up to $30°C$) for erbium oxide. For the other wavelength pairs, its maximal temperature error drops to only $5 - 6°C$. Except the erbium oxide case for λ_1-λ_2, the maximal temperature error still varies as much as 100% (between $10°C$ and $20°C$), depending on the wavelength pairs. With the best wavelength pairs λ_1-λ_3 (see Fig. 8 (a)), the maximal temperature error remains around $10°C$. With the other wavelength pairs, the maximal error is around $20°C$.

In addition, with bichromatic thermoreflectometry method, the temperature error is never canceled and it is always at least equal to $1°C$. For metallic materials, especially for inconel, with a low variation

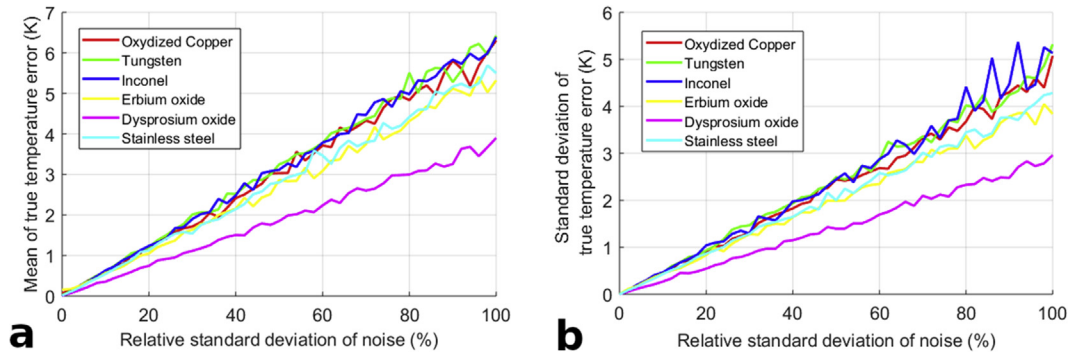

Fig. 6. The mean value ($\bar{E}_T$) (a) and the standard deviation (σ_{E_T}) (b) of temperature error as a function of the normalised standard deviation $\sigma_{I_{rel}}$ with the wavelengths combination: $\lambda_1 = 1.064$, $\lambda_2 = 1.31$ and $\lambda_3 = 1.55\mu m$.

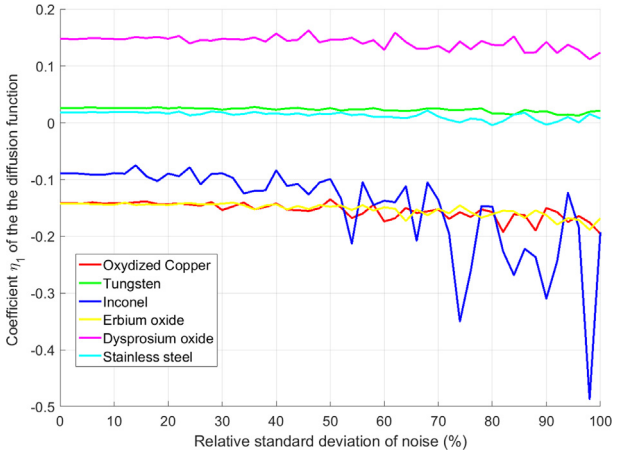

Fig. 7. Coefficient η_1 of the diffusion function modelling $\hat{\eta} = \eta_0 + \eta_1 \times \lambda$.

of the inputs versus the wavelength, the modelling of the diffusion function with a linear function decreases the temperature error. The trichromatic thermoreflectometry thus provides a lower temperature error. For dielectric materials (erbium and dysprosium oxides), with a high variation of inputs versus the wavelength, the temperature error with bichromatic thermoreflectometry can become similar to one obtained by trichromatic thermoreflectometry.

As for the trichromatic themoreflectometry method, the bias on the temperature error increases linearly with the normalised standard deviation $\sigma_{I_{rel}}$ on the inputs. The error temperature would be an amplification of the errors on the inputs. The value of the amplification depends on the value condition number of the Jacobian matrix of the system of radiometric equation (8) calculated in the next subsection.

For the bichromatic thermoreflectometry $\lambda_1 = 1.064$, $\lambda_3 = 1.55\mu m$, method with the best results on temperature error, Fig. 9 displays on the N trials the mean value $\bar{E}_\eta$ of the absolute diffusion function error $E_\eta = ||\eta(\lambda_1) - \hat{\eta}||$.

As for the temperature error, the mean value of the diffusion function error $\bar{E}_\eta$ does not go to zero for a null value on the normalised standard deviation $\sigma_{I_{rel}}$. In the same way, the mean value of diffusion factor error increases linearly with the standard deviation on the noise of the inputs. This error is as high as the condition number, as explained in the next subsection.

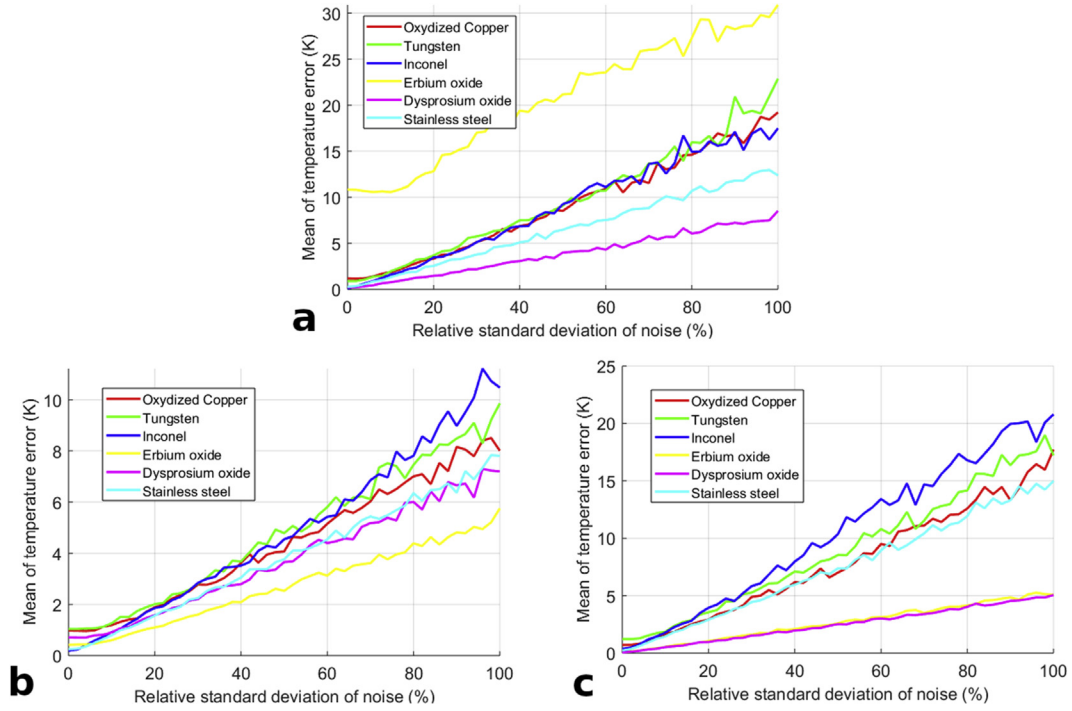

Fig. 8. The mean value of temperature error $\bar{E}_T$ as a function of the normalised standard deviation $\sigma_{I_{rel}}$ on the inputs.

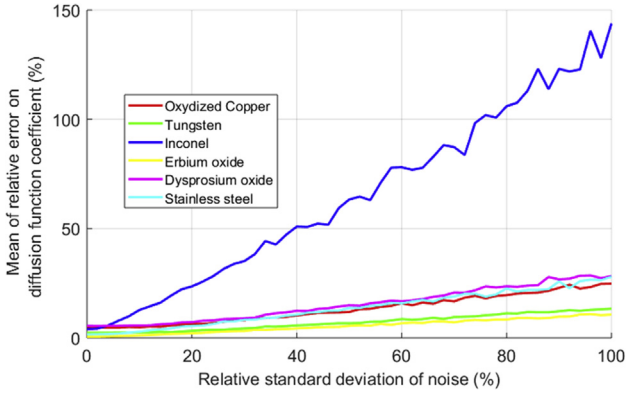

Fig. 9. The mean value of diffusion factor error $\bar{E}_\eta$ as a function of the normalised standard deviation $\sigma_{I_{rel}}$ on the inputs for the bichromatic thermoreflectometry $\lambda_1 - \lambda_3$.

3.4. Condition number analysis for bi- and trichromatic thermoreflectometry method

The differences between the mean value ($\bar{E}_T$) of temperature error between the different methods and the different wavelength pairs for the bi- and trichromatic thermoreflectometry method can be explained, at least partially, by an analysis of the condition number of the Jacobian matrix ($\mathrm{J}(x^\star)$) at the solution (local minimum $x^\star$) of the system explained by radiometric equation (8). This matrix depends on the system observable data (radiance temperature (T_{R_i}) and bidirectional reflectivity ($\rho_i^{\vec{x_0},\vec{r_0}}$) and wavelength ($\lambda_i$) with $i = 1...n$). The computation of Jacobian matrix ($\mathrm{J}(x^\star)$) is directly achieved by using the Matlab algorithm 'fsolve' (with the Trust Region Dogleg algorithm). The condition number of $\mathrm{J}(x^\star)$ expresses the local stability at a neighbourhood $\mathscr{V}_{x^\star}$ of $x^\star$ if it is considered the first-order Taylor expression:

$$\|f(x^\star + h) - f(x^\star)\| \leq \|\|\mathrm{J}(x^\star)\|\|.\ \|\|h\|\| \quad \forall\ h \in \mathscr{V}_{x^\star} \tag{14}$$

where $\|\|\|\|$ is the norm operator matrix. Thus, $\|\|\mathrm{J}(x^\star)\|\|$ locally represents the variation of f. A large condition number shows that the matrix is poorly conditioned and the calculations become very sensitive to the slightest error of the observables (T_{R_i}, $\rho_i^{\vec{x_0},\vec{r_0}}$, λ_i)). A small change in the coefficient matrix can lead to large changes in the outputs (true temperature (T) and coefficients of the diffusion function (η_0 and η_1)). The condition number then gives an idea of how the relative error of the outputs increases during the system resolution.

Fig. 10(a) displays the mean value ($\bar{E}_T$) for each material, each method and for a given value of the normalised standard deviation $\sigma_{I_{rel}} = 15\%$. Fig. 10(b) gives the associated condition number of the Jacobian matrix for each case.

The condition number is the smallest for trichromatic thermoreflectometry method and the mean value ($\bar{E}_T$) of temperature error is also the smallest. In addition, the bichromatic thermoreflectometry methods have the lowest mean value ($\bar{E}_T$) of temperature error and the lowest condition number for a far-distance of wavelength pair and for materials with a small variation in diffusion function and a fairly large variation of emissivity (see Figs. 3 and 1 for tungsten and erbium Oxide). These cases respect the hypothesis of spectral invariance of diffusion function. In addition, a large variation of the inputs over the wavelength range is observed (see Fig. 5). Even with a respected assumption of an almost constant diffusion function on the temperature range, the mean value ($\bar{E}_T$) of both the temperature error and the condition number increase when the variations of the inputs over the wavelength range decrease (see Figs. 1, 3 and 5 for inconel material). This is especially true for erbium oxide with a bichromatic thermoreflectometry method operating with the wavelength pair λ_1-λ_2. For materials with a higher variation of the diffusion function (oxidized copper, stainless steel and dysprosium and erbium oxides), the lowest error temperature corresponds to the lowest condition number. The part of the temperature error resulting from the condition number is higher than the temperature error resulting from the non respect of the hypothesis of a constant diffusion function. This result is consistent with those of the literature [15] for polychromatic methods, where the choice of wavelengths influences the temperature error. The two wavelengths need to be close enough to respect the hypothesis of invariance of the diffusion function and far enough at each other to optimise the system conditioning of equation (8) with a significant difference between its inputs. The high variation of the inputs at two wavelengths is favourable to the decrease of the temperature error. Finally, a low condition number helps to limit the error on the modelling of the diffusion function. The resolution of the system with three equations also fully benefits from value differences between inputs over the wavelength.

3.5. Contributions of trichromatic thermoreflectometry method

For metallic materials (inconel, tungsten and oxidised copper), bichromatic thermoreflectometry with a choice of two distant wavelengths, typically λ_1-λ_3, favours the conditioning of the system and limits the increase of temperature error versus the noise added to the inputs. Trichromatic thermoreflectometry, which improves the modelling of the diffusion function with the wavelength, makes it possible to reduce the temperature error by a percentage of 66%. A temperature

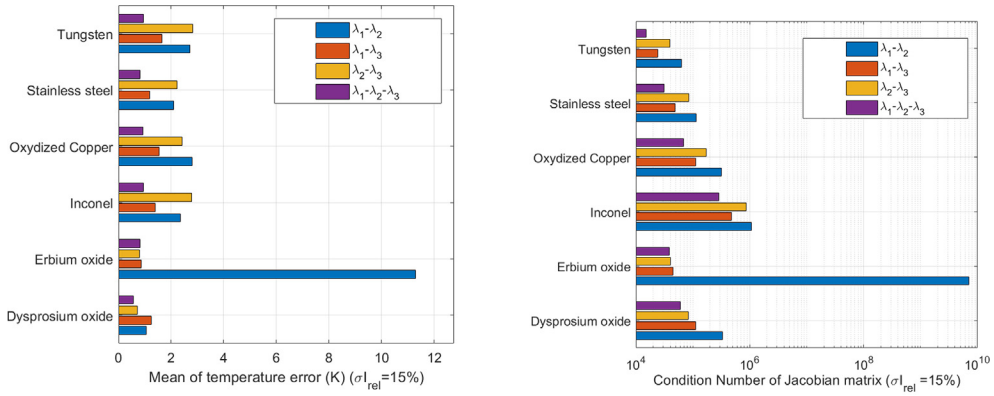

(a) $\bar{E}_T$ (b) Condition number

Fig. 10. The mean value ($\bar{E}_T$) (a) of temperature error and the condition number of the Jacobian matrix for each material of the data base and for each thermoreflectometry method (trichromatic with the wavelengths $\lambda_1 = 1.064$, $\lambda_2 = 1.31$ and $\lambda_3 = 1.55\mu m$ and bichromatic with the wavelength pairs: λ_1-λ_2; λ_1-λ_3 and λ_2-λ_3) for the value of 15% of the normalised standard deviation ($\sigma_{I_{rel}} = 15\%$).

error below $1°C$ can be achieved with a noise standard deviation of less than 15%, which corresponds to a standard deviation on the radiance temperature (and respectively the bidirectional reflectivity) of $0.75°C$ (and respectively of 0.0015 sr^{-1}).

For dielectric materials, the temperature error with bichromatic thermoreflectometry with a choice of two distant wavelengths, λ_1-λ_3, is divided by two with respect to the temperature error on metallic materials. However, trichromatic thermoreflectometry also reduces the temperature error, in particular for Dysprosium oxide, by a better conditioning of the system.

In conclusion, trichromatic thermoreflectometry makes it possible to optimise all measurement situations, and this is verified in a real experiment on a multi-material part in the following section.

4. Experimental performances of true temperature field measurement with bi- and trichromatic thermoreflectometry on a multi-material part

This section compares true temperature field measurements performed with bi- and trichromatic thermoreflectometry on a multi-material part composed of three material samples included in the previous database.

The section begins with the presentation of the thermoreflectometer and the multi-material part. The true temperature measurement is then carried out on each sample by tri- and bichromatic thermoreflectometry using three combinations of wavelengths. The performances, depending on the wavelengths chosen and the studied sample, are detailed and compared between bi- and trichromatic thermoreflectometry.

4.1. Thermoreflectometer presentation

The near-infrared thermoreflectometer in Fig. 11 includes an illuminator based on laser sources, a filter wheel, a near-infrared camera and a data acquisition and control system.

Reflectivity measurement is enabled by three near-infrared lasers centred on wavelengths $\lambda_1 = 1.064$, $\lambda_2 = 1.310$ and $\lambda_3 = 1.550\,\mu m$. Each laser is individually controllable and modulable from 0 to 50 mW. The monochromatic rays at each wavelength are optically coupled into a single optical fibber, and emerge from the same beam expander. Thanks to this enlargement, a 5 cm diameter collimated beam is provided at a distance of $1m$.

The filter wheel is motorised, controllable and selects the spectral band of the camera. The filters mounted on it are centred at a wavelength of 1.064 or 1.310 or 1.550 μm with a bandwidth of 50 nm. The camera is a near-infrared camera equipped with a *InGaAs* detector with a pixel resolution of 320×256 pixels. The Digital Levels (DL) of the camera signal are expressed over 12 bits. Its spectral response ranges from 0.9 to $1.7\mu m$. The control of integration time (ti), between $1\mu s$ and $1s$, enables the acquisition of a high dynamic range of measurement. The camera is then configured in such a way that it avoids a signal level lower than the noise level and the overexposure of the detector. The camera is equipped with a 50 mm focal length lens. The field of view of the camera is around 13×10 cm and the projection of one pixel on the object surface is 0.4 mm. The data acquisition system controls the position of the filter wheel and supplies voltage to the laser sources. It also acquires camera images for radiance temperature and bidirectional reflectivity measurements. The camera images and the radiometric and reflectometric calibration procedure used to relate the images to radiance temperature and bidirectional reflectivity fields are detailed in article [19].

The thermoreflectometer is located approximately at a distance of 1 m, with a viewing angle of 13° with respect to the normal of the sample. The lasers emit with the same angle in order to obtain a maximum reflected signal (Snell-Descartes's conditions). Measurements of radiance temperature and bidirectional reflectivity are carried out at three wavelengths $\lambda_1 = 1.064$, $\lambda_2 = 1.310$ and $\lambda_3 = 1.550\mu m$.

4.2. Multi-material part presentation

The multi-material part, shown in Fig. 12, is composed of three material samples chosen from the previous database. In relation to the results of Figs. 6 and 8, it consists of only one metallic material (the behaviour of metallic materials are similar regarding the methods of thermoreflectometry) and two dielectric materials that have specific behaviours according to the methods used. The samples are heated, under air, on their rear face by a hot plate. The reference temperature, given by a thermocouple welded on the metallic sample and stuck onto dielectric samples, is $500°C$.

The metallic material selected is a roughened stainless steel ($R_a = 5.4\mu m$), slightly oxidised. Its thickness is 3 mm and its diameter is 20 mm. Among the metallic materials, Stainless Steel was chosen for its important spectral variations of emissivity (see Fig. 1) and for its low capacity to oxidise (unlike Tungsten). The dielectric samples are stainless steel substrate coated with a $200\mu m$ layer of zirconia powders mixed with dysprosium oxide ($YSZ + Dy_2\,O_3$) and Erbium oxide ($YSZ + Er_2\,O_3$) deposited by a Plasma Spray Process. As shown in Fig. 1, these materials are challenging for thermography methods because emissivity varies a lot and decreases and increases respectively with the wavelength. The improvements brought by bichromatic thermoreflectometry should be significant, but very dependent on the combination of wavelengths (see Fig. 8).

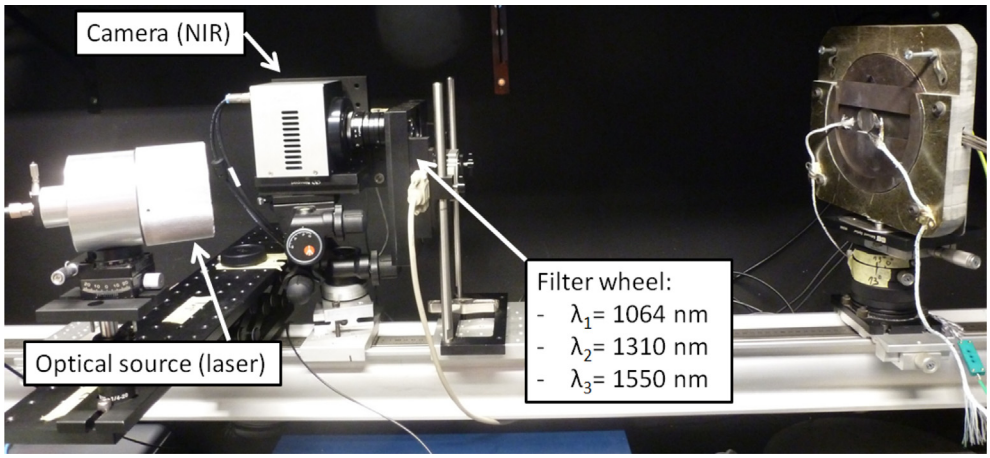

Fig. 11. Thermoreflectometer composed of laser sources, a filter wheel and a near-infrared camera.

Fig. 12. Multi-material part: on the left is a sample of stainless steel substrate coated with a 200μm layer of zirconia powders mixed with dysprosium oxide ($YSZ + Dy_2\ O_3$), in the middle is the stainless steel sample, and on the right is a sample of stainless steel substrate coated with a 200μm layer of zirconia powders mixed with the Erbium oxide ($YSZ + Er_2\ O_3$).

4.3. Temperature field measurements by bi- and trichromatic thermoreflectometry

This sub-section is dedicated to the measurement of true temperature fields on the multi-material part using bi- and trichromatic thermoreflectometry.

4.3.1. Overview of thermoreflectometry: inputs and outputs

The first step of the thermoreflectometry consists in measuring the radiance temperature ($T_R^{\overrightarrow{r0}}(\lambda_i, u, v)$) and the bidirectional reflectivity field ($\rho^{\overrightarrow{x0},\overrightarrow{r0}}(\lambda_i, u, v)$) at each wavelength λ_i (u and v are pixel coordinates). As the temperature is constant, these values are averaged over $N = 50$ images and are noted $\overline{T}_R^{\overrightarrow{r0}}(\lambda_i, u, v)$ and $\overline{\rho}^{\overrightarrow{x0},\overrightarrow{r0}}(\lambda_i, u, v)$.

The outputs of thermoreflectometry are the true temperature field $\hat{T}(u, v)$ and the diffusion function field $\hat{\eta}(u, v)$ with its parameters $\eta_0(u, v)$ and $\eta_1(u, v)$. These outputs are calculated by solving the equation system (8) for the three combinations of wavelengths for bichromatic thermoreflectometry and for trichromatic thermoreflectometry.

To reduce the number of resulting data in this article, the field measurements are provided for only one material (Dysprosium Oxide). For the other ones, a spatial average is calculated, noted $T_R^{\overrightarrow{r0}}(\lambda_i)$, $\rho^{\overrightarrow{x0},\overrightarrow{r0}}(\lambda_i)$, $\hat{T}$ and $\hat{\eta}$ over the pixels belonging to the Region Of Interest (ROI).

4.3.2. Performance criteria

The evaluation of the method is based on the comparison between the reference temperature provided by a thermocouple $T^* = 500°C$ and the estimated one measured by bi- and tri-chromatic thermoreflectometry $\hat{T}$. This temperature criterion ΔT is expressed as follows:

$$\Delta T = \begin{cases} |T^* - \hat{T}(\lambda_i, \lambda_j)| \text{ with } \lambda_i \text{ and } \lambda_j \text{ : pairs of wavelengths} \\ \qquad \text{for bichromatic thermoreflectometry} \\ |T^* - \hat{T}(\lambda_1, \lambda_2, \lambda_3)| \text{ for trichromatic thermoreflectometry} \end{cases} \tag{15}$$

Finally, a temperature score S_T, is established from the temperature criterion in order to draw conclusions on the performances of each thermoreflectometry method. It calculates the average value of the temperature criterion over M materials tested for each thermoreflectometry setting. It is expressed as follows:

$$S_T = \frac{\sum_{i=1}^{M} \Delta T_i}{M} \tag{16}$$

4.3.3. Thermoreflectometry inputs: measurements of radiance temperatures and bidirectional reflectivities

This section presents the results obtained on the inputs of thermoreflectometry, i.e. the radiance temperature field $T_R^{\overrightarrow{r0}}(\lambda_i, u, v)$ and $\rho^{\overrightarrow{x0},\overrightarrow{r0}}(\lambda_i, u, v)$. Fig. 13 displays the radiance temperature and the bidirectional reflectivity field at $\lambda = 1.31\mu m$ for the Dysprosium part.

The mean value of the radiance temperature field at $1.31\mu m$ is $496°C$ and is very homogeneous (less than 0.5% of spatial variations). This high value of radiance temperature is consistent with the high value of emissivity at this wavelength (see Figs. 1 and 5). For the bidirectional reflectivity field, the values are more scattered (8%) around an average of $0.02sr^{-1}$, which is in agreement with Fig. 5. The spatial and temporal averaged radiance temperature $\overline{T}_R^{\overrightarrow{r0}}(\lambda_i)$ and bidirectional reflectivity $\overline{\rho}^{\overrightarrow{x0},\overrightarrow{r0}}(\lambda_i)$ at different wavelengths $\lambda_1 = 1.064$, $\lambda_2 = 1.31$ and $\lambda_3 = 1.55\,\mu m$ are summarised in Fig. 14.

For the stainless steel sample, the values of spatial and temporal averaged radiance temperatures $\overline{T}_R^{\overrightarrow{r0}}$ decrease monotonously with wavelength. The evolution is consistent with the emissivity decrease for metals (see Fig. 1). The values of spatial and temporal averages of bidirectional reflectivities increase with wavelength in accordance with the emissivity decrease and with equation (5). The rather high values are evidence of a quasi-specular material.

For the dielectric samples (Erbium and Dysprosium oxides), the values of spatial and temporal averaged radiance temperatures vary greatly with wavelength, with non-monotonous variations. These variations are consistent with the emissivity spectral variations, presented in Fig. 1. Erbium oxide shows a maximum of radiance temperature at $1.55\mu m$ and Dysprosium oxide at $1.31\mu m$. The values of the spatial and temporal averaged bidirectional reflectivities are quite low, which is consistent with a quasi-lambertian reflector. The spectral variations are inverse compared to the emissivity variations, in accordance with equation (5).

4.3.4. Thermoreflectometry outputs: calculation of true temperature and diffusion function

Once the bidirectional reflectivity and radiance temperature fields are measured, the values of true temperature and diffusion function are calculated by solving the system introduced in equation (8) with two radiometric equations (combinations of two wavelengths) for bichromatic thermoreflectometry and three radiometric equations for trichromatic thermoreflectometry. Fig. 15 displays the true temperature and the diffusion function field for the wavelength couple ($\lambda_1 - \lambda_2$) and for the Dysprosium Oxide part.

The true temperature field mean value is 500. 2°C, which is very close to the thermocouple reference value of 500°C, and the spatial

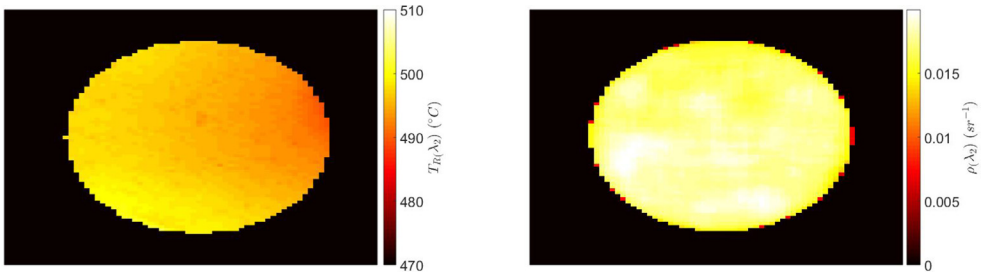

Fig. 13. Inputs of thermoreflectometry for the Dysprosium Oxide part at $1.31\mu m$: a) Radiance temperature field; b) Bidirectional reflectivity field.

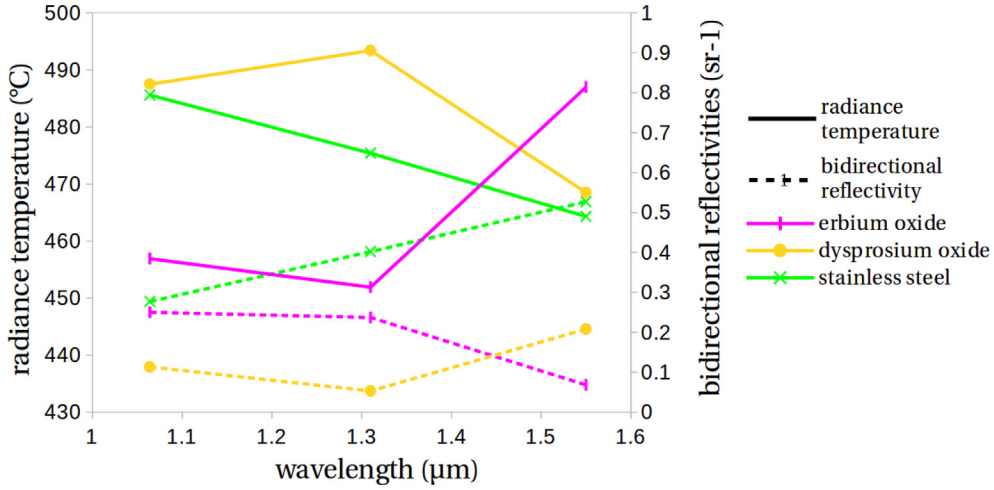

Fig. 14. Spatial and temporal averages of radiance temperature and bidirectional reflectivities for the three wavelengths.

variations are around 8%. The diffusion function value is equal to $2.08sr$, which is close to the value provided in Fig. 3, and exhibit a spatial variation of about 8%. This strong variation can be explained by the propagation of the heterogeneity of the bidirectional reflectivity field to the diffusion function field.

Fig. 16 presents the true temperature field and the diffusion function value at $1.31\mu m$ for trichromatic thermoreflectometry.

The field of true temperature (resp. diffusion function at $1.31\mu m$) exhibit a mean value of 500. $1°C$ (resp. $2.545sr^{-1}$). These values are close to the reference thermocouple value for the true temperature and a bit higher than the spectrometry ones for the diffusion function (see. Fig. 5). The homogeneity of these fields are similar to the one for the bichromatic case.

The spatial and temporal averaged value of true temperature, $\hat{T}$, and diffusion function, $\hat{\eta}$, are gathered in Table 1. According to equation (9) for the bichromatic thermoreflectometry (resp. according to equation (11) for trichromatic thermoreflectometry), the diffusion function is calculated for each wavelength pair (resp. for each wavelength). Table 1 also provides the estimated emissivity $\hat{\vec{r_0}}$ by applying equation (5) with the bidirectional reflectivity $\bar{\rho}^{\overrightarrow{x_0},\overrightarrow{r_0}}$ of Fig. 14 and the diffusion function $\hat{\eta}^{\overrightarrow{r_0},\overrightarrow{x_0}}$ calculated by thermoreflectometry.

As demonstrated for the metallic materials in Fig. 8 (a), (b) and (c), the error on the stainless steel sample true temperature is never zero with the bichromatic methods. Depending on the noise levels on the radiance temperature and the reflectivity measurements, and on the bichromatic thermoreflectometry methods used, this error can vary. The maximal true temperature error is recorded for the wavelength combination λ_2-λ_3. On the other hand, as shown in Fig. 6, it is expected that this true temperature error should become very small for the trichromatic thermoreflectometry method. The true temperature calculated is very close to the reference temperature of $500°C$.

Similarly, the difference between the diffusion function calculated and the diffusion function values plotted in Fig. 3 is higher with the bichromatic thermoreflectometry method than with the trichromatic one. Indeed, the value of the diffusion function obtained with trichromatic thermoreflectometry is centred around $0.93\ sr^{-1}$. This value is very consistent with the trend observed in the spectrometer results in Fig. 3, even if the spectral variations observed on the trichromatic method are a decrease, instead of an increase for spectrometry. This could be due to residual oxidation, which modifies the optical index at the surface, affecting the diffusion function spectral variations. Nevertheless, these low values of the diffusion function still testify to the rather specular behaviour of the sample.

Finally, the values of the emissivities deduced by thermoreflectometry are comparable with those measured by the spectrometer (see Fig. 1) and these values also decreased with the wavelength. The comparison of the values of emissivity obtained with two very different apparatus (spectrometer and thermoreflectometer) in different conditions greatly reinforces the overall consistency of the thermoreflectometry method.

For the dielectric samples (Erbium and Dysprosium oxides), except for Erbium oxide with the bichromatic thermoreflectometry method with the combination λ_1-λ_2, which introduces outliers on true temperature and diffusion function, as expected in Fig. 8 (a), (b) and (c), the true temperature error is very low with the four methods. The true temperatures calculated are close to each other and close to the reference temperature of $500°C$. For Erbium oxide with the bichromatic thermoreflectometry method with the combination λ_1-λ_2, the close values of radiance temperature and bidirectional reflectivity at both wavelengths lead to a bad conditioning of the equations system (8).

Comparing the calculated values of the diffusion factor with the ones of Fig. 3, we can conclude that the difference is also very small. Some small differences exist in the spectral variations between thermoreflectometry and spectrometry, and this could be explained by the effect of temperature on the optical index, which can be important for ceramic materials. The high values of the diffusion function show a

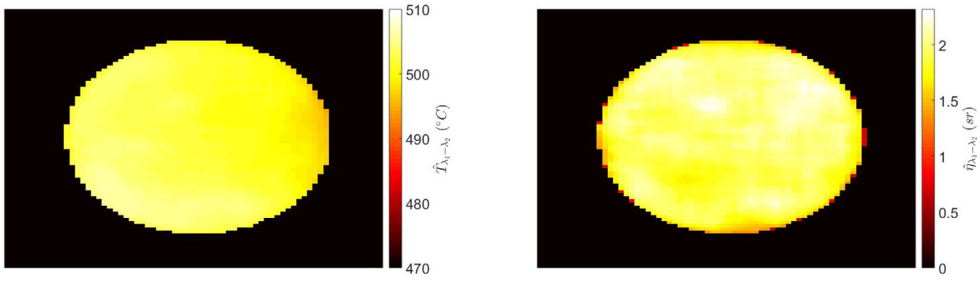

Fig. 15. Outputs of bichromatic ($\lambda_1 - \lambda_2$) thermoreflectometry for the Dysprosium Oxide part: a) True temperature field; b) Diffusion function field.

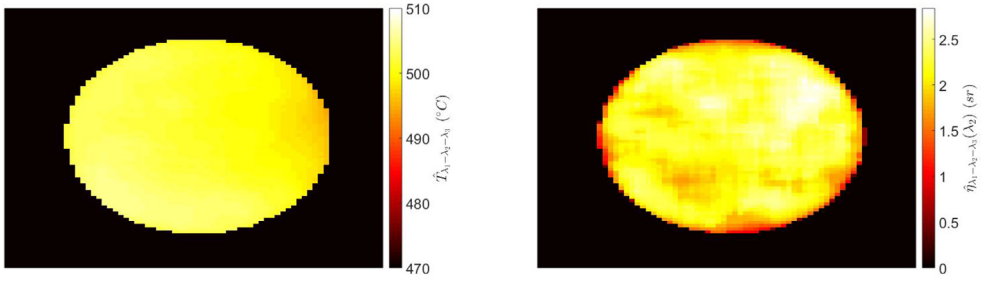

Fig. 16. Outputs of trichromatic thermoreflectometry for the Dysprosium Oxide part: a) True temperature field; b) Diffusion function field at $1.31\mu m$.

Table 1
Spatial and temporal averaged value of true temperature, diffusion factors and emissivities for the bichromatic methods (with the three possible combinations of wavelengths: λ_1-λ_2, λ_1-λ_3, λ_2-λ_3) and trichromatic thermoreflectometry (λ_1-λ_2-λ_3).

Outputs	Method	Wavelength	Stainless steel	Erbium oxide	Dysprosium oxide
$\hat{T}$ $(°C)$	λ_1–λ_2	–	497.1	**487.8**	500.2
	λ_1–λ_3	–	495.9	499.0	497.3
	λ_2–λ_3	–	493.1	499.1	499.1
	λ_1–$\lambda_2\lambda_3$	–	500.1	500.1	499.5
$\hat{\eta}^{\overrightarrow{r_0},\overrightarrow{x_0}}$ (sr)	λ_1–λ_2	–	0.841	**2.26**	2.24
	λ_1–λ_3	–	0.766	2.543	1.798
	λ_2–λ_3	–	0.715	2.545	1.878
	λ_1–$\lambda_2\lambda_3$	λ_1	1.026	2.544	2.13
		λ_2	0.931	2.545	2.01
		λ_3	0.838	2.547	1.89
$\hat{\varepsilon}^{\overrightarrow{r_0}}$	λ_1–λ_2	λ_1	0.77	**0.43**	0.75
		λ_2	0.66	**0.46**	0.88
	λ_1–λ_3	λ_1	0.79	0.36	0.80
		λ_3	0.60	0.83	0.62
	λ_2–λ_3	λ_2	0.71	0.40	0.90
		λ_3	0.63	0.83	0.61
	λ_1–λ_3	λ_1	0.72	0.36	0.76
		λ_2	0.63	0.40	0.89
		λ_3	0.56	0.83	0.61

diffuse and quasi-lambertian behaviour, still in accordance with the spectrometer results.

Similarly, the calculated emissivity values are very close to those measured by the spectrometer (see Fig. 1). Finally, all combinations of wavelengths for all the methods are very consistent and provide an accurate value of true temperature and diffusion function.

4.3.5. Calculation of the temperature criterion

From the reference temperature $T^* = 500°C$ and the temperatures calculated above, the temperature criterion is calculated applying equation (15) for each thermoreflectometry setting and material. The values are displayed in Table 2.

With regard to the stainless steel sample, the criterion is around $1.2°C$ for bichromatic thermoreflectometry with couples λ_1-λ_2 and λ_1-λ_3 and reaches $3°C$ for the configuration λ_2-λ_3. These high values of the criterion can be explained by a non-optimal mathematical conditioning

Table 2
Temperature criterion for each thermoreflectometry method, wavelength choice and material.

Method	$\Delta T\,(°C)$		
	Stainless steel	Erbium oxide	Dysprosium oxide
λ_1–λ_2	0.9	19.1	0.7
λ_1–λ_3	1.5	0.6	2.4
λ_2–λ_3	3.0	1.5	0.9
λ_1–$\lambda_2\lambda_3$	0.1	0.1	0.5

of system (8) at these wavelengths. However, for trichromatic thermoreflectometry, the error clearly tends to 0. We can conclude that on this kind of metallic material, trichromatic thermoreflectometry provides an improvement of the true temperature measurement accuracy compared to the bichromatic thermoreflectometry.

For the Dysprosium oxide case, every method is almost equally reliable and involves a criterion inferior to $1°C$. Only the configuration λ_1-λ_3 leads to a criterion around $2.4°C$. For the Erbium oxide case, the strongest radiance temperature errors are recorded for configuration λ_1-λ_2 and almost reach $19°C$. Once again, and as noticed in previous parts, this is due to a non-optimal mathematical conditioning caused by the couple wavelength/emissivity, which leads to high radiance temperature error.

4.3.6. Calculation of the temperature score

The temperature score S_T is calculated from equation (16) and from the temperature criterion values shown in Table 2, with $M = 3$ materials. For each thermoreflectometry method, the values of the temperature score are displayed in Fig. 17.

The comparison of the performances of each method over a range of material indicates that trichromatic thermoreflectometry is the most accurate and flexible method. The global error is around $0.2°C$ at $500°C$ for this configuration. Bichromatic thermoreflectometry also provides satisfying results for configurations λ_1-λ_3 and λ_2-λ_3, but shows higher errors for λ_1-λ_2. These results, obtained on three selected materials covering the quasi-entire range of emissivities (see Fig. 1), reinforce the physical consistency of the thermoreflectometry method. This method can thus be trusted as a true temperature measurement method, but it can also provide a reliable in-situ continuous estimation of emissivity at two or three near-infrared wavelengths.

5. Conclusion

This article demonstrated that trichromatic thermoreflectometry introduced a lower temperature error than bichromatic

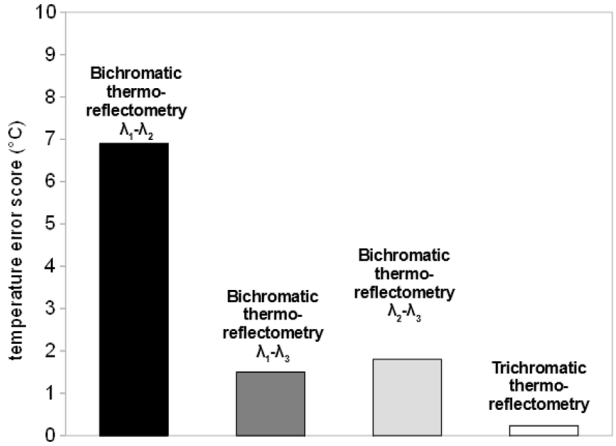

Fig. 17. Temperature error scores for each method and configuration.

thermoreflectometry for measuring true temperature fields on a multi-material part. The true temperature field is obtained thanks to simultaneous measurements at two or three wavelengths of the radiance temperature field and the bidirectional reflectivities field and by the resolution of a system of two or three radiometric equations based on the modelling of the spectral evolution of the diffusion function. These methods are applied to opaque and various spectral behaviours of metallic and dielectric materials whose emissivity is different over wavelength and time.

Section 2 discussed the diffusion function modelling from a database of thermo-optical properties of these various spectral behaviours of six metallic and dielectric materials. The database includes emissivity and diffusion function measurements performed at room temperature using a FTIR spectrometer equipped with different accessories. Some materials exhibit a low variation of the diffusion function with the wavelength, less than 1%, and a modelling defined as a constant value relative to the wavelength was found suitable. This modelling corresponds to bichromatic thermoreflectometry. For materials with a diffusion function variation higher than 1%, a linear function of the wavelength is required and thus trichromatic thermoreflectometry was set up. The main advantage of the thermoreflectometry method is that by using a simple linear function for modelling the diffusion function, all cases of emissivity behaviours are addressed. A system with a maximum of three radiometric equations solves all cases of non-contact measurement of opaque materials.

Section 3 performed an analysis on the propagation of uncertainties of bi- and trichromatic thermoreflectometry on simulated data resulting from the database of previous materials. For a given standard deviation of noise, 500 noisy inputs (radiance temperature and bidirectional reflectivity) were generated and five hundred estimations of the outputs (temperature and diffusion function) were proceeded. The temperature error between the reference temperature of simulation and the estimated one, averaged on the five hundred trials, was calculated. The trichromatic thermoreflectometry exhibits a temperature error that is twice lower for materials with a diffusion function variation higher than 1%. The introduced model of the diffusion function enables to take into account the physical variations of the diffusion function with wavelength. The error on the estimated temperature is thus reduced. For other materials with a low variation of the diffusion function, trichromatic thermoreflectometry also minimises the temperature error thanks to the introduction of a third wavelength, which improves the convergence of the resolution method of the system of radiometric equations. Moreover, the temperature error depends on the choice of the wavelength pairs for bichromatic thermoreflectometry. In all materials cases, the temperature error increases linearly with the standard deviation on noise inputs. However, the slope of the plot between the temperature error and the noise standard deviation depends on the material (i.e the sensitivity of the diffusion function model to the estimated parameter at selected wavelength) and the choice of the wavelength pairs for bichromatic thermoreflectometry. The value of the slope is always lower for trichromatic thermoreflectometry which demonstrates its better robustness. Finally, trichromatic thermoreflectometry has the capability to achieve a residual temperature error of less than one degree, whatever the spectral behaviour of the materials.

Section 4 measured true temperature fields on a part with three of the six preceding materials found in the database, one metal (stainless steel) and two dielectric (zirconia powder mixed with either dysprosium oxide or erbium oxide). This true temperature is performed by tri- and bichromatic thermoreflectometry using the different pairs of wavelengths. This experiment showed that bichromatic thermoreflectometry with the wrong choice of wavelength pairs does not provide the right true temperature on materials with low and same variations in the measurement of radiance temperature and bidirectional reflectivity. However, for materials with large and opposite variations in radiance temperature and bidirectional reflectivity, bichromatic and trichromatic thermoreflectometry give similar true temperatures. Finally, for materials with small and opposite variations in radiance temperature and bidirectional reflectivity measurements between different wavelengths, trichromatic thermoreflectometry improves the true temperature measurement. Finally, the diffusion factor and emissivity values estimated by the trichromatic thermoreflectometry are consistent with the measurements performed with the spectrometer FTIR in section 2. This demonstrates the physical consistency of the results obtained with the trichromatic thermoreflectometry.

The work in progress deals with a physical modelling of the diffusion function. This modelling will be based on a physical model of the Bidirectional Reflectivity Distribution Function (BRDF). This model will take into account the surface properties of the material (roughness and optical indices) and the geometric configuration of the thermoreflectometer. Measurements will be provided, in situ and in real time, of both true temperature and surface properties, through the estimation of roughness and optical indices.

References

[1] X. Courtois, M. Aumeunier, M. Joanny, H. Roche, F. Micolon, S. Salasca, C. Balorin, M. Jouve, IR thermography diagnostics for the WEST project, Fusion Eng. Des. 89 (9–10) (2014) 2472–2476.

[2] M.M. Gentleman, V. Lughi, J.A. Nychka, D.R. Clarke, Noncontact methods for measuring thermal barrier coating temperatures, Int. J. Appl. Ceram. Technol. 3 (2) (2006) 105–112.

[3] J. Thevenet, M. Siroux, B. Desmet, Measurements of brake disc surface temperature and emissivity by two-color pyrometry, Appl. Therm. Eng. 30 (6–7) (2010) 753–759.

[4] M. Kuball, G.J. Riedel, J.W. Pomeroy, A. Sarua, M.J. Uren, T. Martin, K.P. Hilton, J.O. Maclean, D.J. Wallis, Time-resolved temperature measurement of algan/gan electronic devices using micro-Raman spectroscopy, IEEE Electron. Device Lett. 28 (2) (2007) 86–89.

[5] M. Vollmer, K.-P. Mollmann, Advanced Methods in IR Imaging, Wiley-VCH Verlag GmbH and Co. KGaA, 2010, pp. 157–237.

[6] B. Rousseau, J.F. Brun, D.D.S. Meneses, P. Echegut, Temperature measurement: christiansen wavelength and blackbody reference, Int. J. Thermophys. 26 (2005) 1277–1286.

[7] C. Cagran, L. Hanssen, M. Noorma, A. Gura, S. Mekhontsev, Temperature resolved infrared spectral emissivity of sic and *pt*-10*rh* for temperatures up to 900°C, Int. J. Thermophys. 28 (2) (2007) 581–597.

[8] T. Pierre, B. Remy, A. Degiovanni, Microscale temperature measurement by the multispectral and statistic method in the ultraviolet-visible wavelengths, J. Appl. Phys. 103 (3) (2008) 34–41.

[9] P. Hagqvist, F. Sikstrom, A.-K. Christiansson, B. Lennartson, Emissivity compensated spectral pyrometry algorithm and sensitivity analysis, Meas. Sci. Technol. 25 (2) (2014) 025011.

[10] O. Riou, P.-O. Logerais, F. Delaleux, J.-F. Durastanti, A self-method for resolving the problem of apparent LWIR emissivity for quantitative thermography up to 130°*c*, Infrared Phys. Technol. 67 (2014) 504–513.

[11] J.L. Gardner, T.P. Jones, Multi-wavelength radiation pyrometry where reflectance is measured to estimate emissivity, J. Phys. E Sci. Instrum. 13 (3) (1980) 306–316.

[12] P. Coates, Multi wavelength pyrometry, Metrologia 17 (3) (1981) 103–110.

[13] H. Madura, M. Kastek, T. Piatkowski, Automatic compensation of emissivity in three-wavelength pyrometers, Infrared Phys. Technol. 51 (1) (2007) 1–8.

[14] T. Duvaut, Comparison between multiwavelength infrared and visible pyrometry: application to metals, Infrared Phys. Technol. 51 (4) (2008) 292–299.

[15] C. Rodiet, B. Remy, A. Degiovanni, Optimal wavelengths obtained from laws analogous to the wien's law for monospectral and bispectral methods, and general methodology for multispectral temperature measurements taking into account global transfer function including non-uniform emissivity of surfaces, Infrared Phys. Technol. 76 (2016) 444–454.

[16] B. Agoudjil, S. Datcu, A. Boudenne, L. Ibos, Y. Candau, Parametric estimation of thermoradiative properties of materials based on harmonic excitation, Rev. Sci. Instrum. 77 (3) (2006) 78–86.

[17] S. Amiel, T. Loarer, C. Pocheau, H. Roche, M.H. Aumeunier, E. Gauthier, C. Le Niliot, F. Rigollet, Surface temperature measurement of plasma facing components with active pyrometry, J. Phys. Conf. Ser. 395 (1) (2012) 012074.

[18] L. Hanssen, C. Cagran, A. Prokhorov, S. Mekhontsev, V. Khromchenko, Use of a high-temperature integrating sphere reflectometer for surface-temperature measurements, Int. J. Thermophys. 28 (2) (2007) 566–580.

[19] T. Sentenac, R. Gilblas, D. Hernandez, Y. Le Maoult, Bi-color near infrared thermoreflectometry: a method for true temperature field measurement, Rev. Sci. Instrum. 83 (12) (2012) 124–136.

[20] R. Gilblas, T. Sentenac, D. Hernandez, Y. Le Maoult, Quantitative temperature field measurements on a non-gray multi-materials scene by thermoreflectometry, Infrared Phys. Technol. 66 (0) (2014) 70–77.